Unmanned Systems, Available online 15 October 2024
DOI:10.1142/S2301385025500748

Cascaded Incremental Nonlinear Dynamic Inversion Trajectory Following For A Stratospheric Airship In Wind

Leo Schneider[a] Toufik Souanef[a*] and James F. Whidborne[a]

[a]*School of Aerospace Transport and Manufacturing, Cranfield University, Cranfield, UK*
**E-mail: toufik.souanef@cranfield.ac.uk*

This paper presents a guidance and control system for controlling the trajectory of a stratospheric unmanned airship using a cascaded Incremental Nonlinear Dynamic Inversion (INDI) method. The control system uses a two-loop cascaded INDI controller with virtual efforts and moments formulation to control both the airship attitude and velocity, while providing perturbation rejection properties. An active-set solver allocates the virtual controls to the airship propellers and aerodynamic surfaces while respecting the actuator bounds and rates saturation. The guidance system uses a Nonlinear Dynamic Inversion controller, where the position error dynamics formulation explicitly considers the lateral velocity of the airship, which enables it to counteract the wind influence. Simulation results demonstrate that the reference trajectory is precisely followed, even in the presence of unknown wind perturbations and both aerodynamic coefficients and mass and inertia parametric uncertainties through Monte-Carlo simulations.

Keywords: Airship, Trajectory-following, Guidance and control, Incremental Non-linear Dynamic Inversion

1. Introduction

Stratospheric airships could potentially become valuable assets for conducting surveillance missions, facilitating military intelligence operations, and enabling long-range communication broadcasting [1]. This potential comes from their extended airborne endurance which can last from days to months or even longer. This endurance, enabled by their lifting hull, introduces a notable drawback: increased susceptibility to wind conditions. As outlined in weather measurement campaigns [2], at an altitude near 21 km, the stratosphere experiences average winds of 10 m/s, occasionally surging beyond 40 m/s. These elevated wind speeds can potentially destabilize airships, complicating trajectory tracking tasks, particularly for those operating in the lower stratosphere. Therefore, it is required to develop guidance and control systems that enable wind-robust trajectory following.

Numerous control methods have been employed to solve the airship trajectory following problem. A path-following controller for airships was proposed using H_∞ and PI control [3]. A path-following control design has been developed by linearising the dynamic model, which is effective near the equilibrium point [4]. In [5] gain scheduled linear quadratic regulators have been proposed. In [6] sliding mode control has shown good performance even with varying wind-speed. A global planar path-following strategy for stratospheric airships was proposed based on guidance integrated backstepping control [7]. A sliding mode control for an autonomous unmanned airship has also been proposed [8]. The research of [9] presented a backstepping controller for airship path-following, considering nonlinear models, external disturbances, and actuator saturation. A path-following controller using backstepping and PD control techniques was developed [10], where the guidance vector is constructed to obtain the desired attitude angles and velocity. A gain-scheduling controller for airship path following under wind disturbances is proposed in [11]. In [12] a command filtered backstepping controller based on the guidance-based path-following principle for underactuated stratospheric airships is introduced.

The planar path-following control problem for autonomous airships was investigated by [13], taking into account actuator saturation, actuator dynamics, parameter variation, and wind fields. The proposed solution combined a command filtered backstepping controller with a nonlinear disturbance observer. In addition, [14] designed a Lyapunov-based guidance law with sideslip and attack angle compensation to reduce path-following steady-state error. Wang [15] proposed a parameter-observer-based LOS (POBLOS) guidance law inspired by the line-of-sight (LOS) guidance law, which estimated and compensated for unknown and time-varying wind influence. Reference [16] introduced a virtual guidance-based finite-time adaptive neural backstepping path-following control approach for underactuated autonomous airships with error constraints and uncertainties.

In [17], adaptive sliding mode control was able to con-

Published by World Scientific. This is the Author Accepted Manuscript issued with: Creative Commons Attribution Non-Commercial License (CC:BY:NC 4.0).
The final published version (version of record) is available online at DOI:10.1142/S2301385025500748. Please refer to any applicable publisher terms of use.

trol a large stratospheric airship in wind, with model parametric uncertainties. To consider explicitly the impact of the wind, [18] have proposed a backstepping sliding-mode controller in pair with a disturbance-observer. Recently, a sliding mode adaptive $\mathcal{L}_1$ controller providing fast adaptation to unknown unsteady wind has been proposed in [19]. Finally, [20] introduced an approach to finite-time trajectory tracking control for multivectored propeller airships, incorporating an incremental backstepping nonsingular terminal sliding mode controller and a nonlinear disturbance observer to achieve stable and precise tracking, even in the presence of uncertainties and unknown disturbances.

It is worth noting that most of the research discussed in these papers primarily examines paths in a two-dimensional plane, but in the presence of wind disturbance, it is more appropriate to consider full three-dimension path-following [19].

The airship dynamics can be inverted using Nonlinear Dynamic Inversion (NDI), as in [21]. NDI requires the airship nonlinear model to be inverted on-board in real-time. In practice, the model is highly uncertain thus reducing the NDI robustness. Therefore to address this limitation, Incremental Nonlinear Dynamic Inversion (INDI) has been developed [22–24]. Unlike NDI, INDI does not rely on a model of the system dynamics but solely on a model of the control dynamics, thereby making it more robust. However INDI requires the assumption that the airship dynamics are slow compared to the control dynamics, but this is the case for large stratospheric airships.

There appears to be just two previous attempts to tackle the airship path following problem using INDI. Firstly, in [25], the lateral dynamics are controlled to guide horizontally an autonomous airship. INDI was applied on a linearised model of the lateral dynamics to control both the roll and yaw rates. Aided by an LQR outer-loop controller, the system ensures effective horizontal path tracking. Simulations demonstrated the system efficacy for path following tasks, even in windy conditions. Despite occasional rudder deflection saturation, the airship performance remains satisfactory. Secondly, in [26], the longitudinal dynamics are controlled to guide an autonomous airship in the vertical plane. Using INDI, a moving gondola controls the airship pitch attitude while propellers control the airship velocity. Simulations with wind gusts have shown that the proposed controller enables robust altitude tracking. But in presence of constant wind there is a small steady state error. This is due to the fact that the wind influence is not explicitly taken into account or that no integral term is used inside the desired position error dynamics.

Neither of the above papers cover the full airship dynamics, both lateral or longitudinal tracking. Hence in this paper, the INDI approach is applied as part of an NDI solution to the trajectory tracking problem for a full six degrees-of-freedom model of a stratospheric airship including wind disturbances. It is evident that consideration of the full airship dynamics yields more accurate representations of the real system behavior compared to controllers relying solely on simplified point mass models or those that consider separated lateral and longitudinal models. By doing so, the design takes into account the full synergy of the systems. This is especially true in the presence of wind, where the maneuvers to keep the system on track are more complicated.

The proposed control solution consists of

(1) an INDI inner-loop that controls the body rates, both in attitude and translation, that is aided by a control allocation scheme that uses an active set solver to distribute the control between the effectors,
(2) an NDI outer-loop attitude controller,
(3) and an NDI guidance controller that ensures trajectory following despite wind.

The contributions of the paper are:

- Introduction of a guidance and control system for a stratospheric unmanned airship employing a cascaded INDI method.
- Implementation of a two-loop cascaded INDI controller with virtual efforts and moments formulation to regulate airship attitude and velocity, while ensuring perturbation rejection properties.
- Application of an active-set solver to allocate virtual controls to airship propellers and aerodynamic surfaces, maintaining adherence to actuator bounds and rates saturation.
- Integration of a Nonlinear Dynamic Inversion controller into the guidance system, wherein the position error dynamics formulation explicitly considers the lateral velocity of the airship, facilitating mitigation of wind influence.

Simulation results demonstrate the precise trajectory tracking even in the presence of unknown wind perturbations and uncertainties in aerodynamic coefficients, mass, and inertia through Monte-Carlo simulations.

The remaining of the paper is organised as follows. In Section 2 the airship model is summarised; details can be found in the references. Section 3 describes the design of the control system. Section 4 presents the guidance system. Section 5 demonstrates the performance of the proposed guidance and control system through simulations. The final section summarises the paper and provides some suggestions for further investigation.

2. Airship model

The kinematic and dynamic model of the airship comes from [27] and [18]. The aerodynamic model comes from [28].

2.1. *Preliminaries*

Assumption 2.1. Throughout cruise flight, the stratospheric airship is neutrally buoyant i.e. the gravity and buoyancy forces compensate themselves: practically this is achieved by controlling the volume of air inside ballonets

placed in the hull. Moreover, both the airship mass and the center of gravity position are slowly varying: ballonets draw in or out air relatively slowly, leading to low rate mass changes. Furthermore, the airship is a rigid body.

The reference frames are shown in Fig. 1 and are:

- $R_E(R, \mathbf{x}_0, \mathbf{y}_0, \mathbf{z}_0)$, the earth inertial reference frame, whose origin R is an arbitrary point, O, located on the earth surface and whose axes are pointing north, east and down respectively.
- $R_b(R, \mathbf{x}_b, \mathbf{y}_b, \mathbf{z}_b)$, the airship body frame, whose origin is the center of volume, C_V. The body frame rotation is parameterised using the Euler angles ϕ, θ, ψ. The centre of gravity is denoted by C_G.

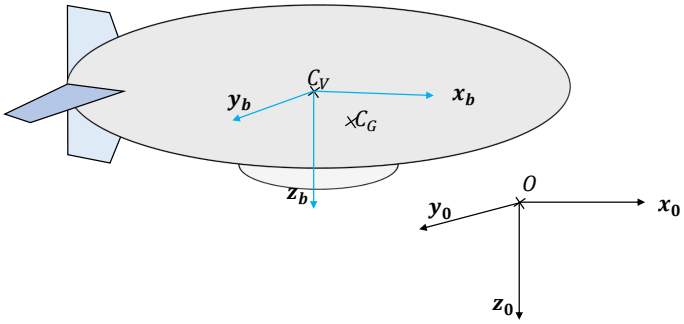


Fig. 1. Stratospheric airship and reference frames

2.2. *Kinematics*

The translational and rotational kinematic model is expressed [27, 29] as:

$$\dot{\mathbf{x}}_1(t) = \mathbf{T}\mathbf{x}_2(t) \tag{1}$$

where $\mathbf{x}_1 = \begin{pmatrix} \boldsymbol{\xi}^T & \boldsymbol{\eta}^T \end{pmatrix}^T$, $\mathbf{x}_2 = \begin{pmatrix} \mathbf{v}_a^T & \mathbf{w}^T \end{pmatrix}^T$ with $\boldsymbol{\xi} = \begin{pmatrix} x & y & z \end{pmatrix}^T$ is the airship center of volume position in the Earth frame, $\boldsymbol{\eta} = \begin{pmatrix} \phi & \theta & \psi \end{pmatrix}^T$ is the attitude vector, $\mathbf{v}_a = \begin{pmatrix} u & v & w \end{pmatrix}^T$ and $\boldsymbol{\omega} = \begin{pmatrix} p & q & r \end{pmatrix}^T$ are the velocities and angular rates in the airship body frame respectively and:

$$\mathbf{T} = \begin{pmatrix} \mathbf{R}(\boldsymbol{\eta}) & 0 \\ 0 & \mathbf{J}(\boldsymbol{\eta}) \end{pmatrix} \tag{2}$$

where the direction cosine matrix $\mathbf{R}$ is:

$$\mathbf{R}(\boldsymbol{\eta}) = \begin{pmatrix} c_\theta c_\psi & -c_\phi s_\psi + s_\phi s_\theta c_\psi & s_\phi s_\psi + c_\phi s_\theta c_\psi \\ c_\theta s_\psi & c_\phi c_\psi + s_\phi s_\theta s_\psi & -s_\phi c_\psi + c_\phi s_\theta s_\psi \\ -s_\theta & s_\phi c_\theta & c_\theta c_\phi \end{pmatrix} \tag{3}$$

where $s_{(\cdot)}$ and $c_{(\cdot)}$ denote sine and cosine functions respectively, and the angular rates transformation matrix $\mathbf{J}$ is:

$$\mathbf{J}(\boldsymbol{\eta}) = \begin{pmatrix} 1 & \sin\phi\tan\theta & \cos\phi\tan\theta \\ 0 & \cos\phi & -\sin\phi \\ 0 & \sin\phi\sec\theta & \cos\phi\sec\theta \end{pmatrix} \tag{4}$$

2.3. *Dynamics*

2.3.1. *Fundamental principle of dynamics*

As in [18, 27], the fundamental principle of dynamics applied at the center of volume of the airship gives:

$$\mathbf{M}_a \begin{pmatrix} \dot{\mathbf{v}}_a(t) \\ \dot{\boldsymbol{\omega}}(t) \end{pmatrix} = \begin{pmatrix} \mathbf{f}_K + \mathbf{f}_{GB} + \mathbf{f}_A + \mathbf{f}_W \\ \mathbf{m}_K + \mathbf{m}_{GB} + \mathbf{m}_A + \mathbf{m}_W \end{pmatrix} + \begin{pmatrix} \mathbf{f}_{CP} \\ \mathbf{m}_{CP} \end{pmatrix} \tag{5}$$

where $\mathbf{M}_a$ is the generalized mass matrix, $\mathbf{f}_K$ is the kinetic force vector, $\mathbf{f}_{GB}$ is the gravity and buoyancy force vector, $\mathbf{f}_A$ is the aerodynamic force vector, $\mathbf{f}_{CP}$ is the control surfaces and propellers force vector, $\mathbf{m}_K$, $\mathbf{m}_{GB}$, $\mathbf{m}_A$ and $\mathbf{m}_{CP}$ are the moments associated with the different forces, and $\mathbf{f}_W$ and $\mathbf{m}_W$ denote the wind disturbance force and moment vectors.

Equation (5) can be rewritten as a control-affine nonlinear system:

$$\dot{\mathbf{x}}_2(t) = \mathbf{f}_2(\mathbf{x}_2) + \mathbf{M}_a^{-1}\mathbf{U}(t) + \mathbf{d}(t) \tag{6}$$

where $U = \begin{pmatrix} \mathbf{f}_{CP}^T & \mathbf{m}_{CP}^T \end{pmatrix}^T$ is the virtual control inputs vector to be defined, $\mathbf{d}(t)$ is an unknown disturbance vector that includes the wind effects, and

$$\mathbf{f}_2 = \mathbf{M}_a^{-1} \begin{pmatrix} \mathbf{f}_K + \mathbf{f}_{GB} + \mathbf{f}_A \\ \mathbf{m}_K + \mathbf{m}_{GB} + \mathbf{m}_a \end{pmatrix} \tag{7}$$

As stated in [28], it is essential to consider the momentum resulting from the fluid displacement around the airship hull for airships. This is because the displaced fluid represents a mass roughly equivalent to the mass of the airship itself.

Hence, $\mathbf{M}_a$ contains two terms:

- the mass and inertia matrix of the airship hull, gondola, payload and propellers
- the added mass and inertia matrix corresponding to the displaced fluid

Both [28] and [27] assumed that the flow around the airship is a potential flow, i.e. steady, incompressible, inviscid and irrotational. In addition, the fluid displacement of the airship is mainly due to the airship hull, thus neglecting the fluid displaced by the gondola.

Under these assumptions, analytical formulas for an double-ellipsoid body [30] are used in [28] to derive the added mass and inertia matrix.

2.3.2. *Control surfaces*

The airship has a two-sided elevator (left and right) and a two-sided (upper and lower) rudder. Their corresponding deflections are denoted δ_{eL}, δ_{eR}, δ_{rU} and δ_{rB}. It is considered that the rudder lateral forces are negligible which

implies that the airship is under-actuated. Hence the control surfaces forces and moments are:

$$\begin{pmatrix}\mathbf{f}_{CP}\\ \mathbf{m}_{CP}\end{pmatrix}_{\text{surf}} = \begin{pmatrix} 0 & 0 & 0 & 0\\ 0 & 0 & 0 & 0\\ \bar{q}S_h\widehat{C}_{z\delta_e} & \bar{q}S_h\widehat{C}_{z\delta_e} & 0 & 0\\ \bar{q}S_hL\widehat{C}_{l\delta_e} & -\bar{q}S_hL\widehat{C}_{l\delta_e} & \bar{q}S_hL\widehat{C}_{l\delta_r} & -\bar{q}S_hL\widehat{C}_{l\delta_r}\\ \bar{q}S_hL\widehat{C}_{m\delta_e} & \bar{q}S_hL\widehat{C}_{m\delta_e} & 0 & 0\\ 0 & 0 & \bar{q}S_hL\widehat{C}_{n\delta_r} & \bar{q}S_hL\widehat{C}_{n\delta_r}\end{pmatrix}\begin{pmatrix}\delta_{eL}\\ \delta_{eR}\\ \delta_{rU}\\ \delta_{rB}\end{pmatrix} \tag{8}$$

where $\bar{q} = \rho V^2/2$ is the dynamic pressure with V the airspeed and ρ the air density, S_h is the hull surface area, L is the hull length, $\widehat{C}_{z\delta_e}, \widehat{C}_{l\delta_e}, \widehat{C}_{l\delta_e}, \widehat{C}_{l\delta_r}, \widehat{C}_{m\delta_e}, \widehat{C}_{n\delta_r}$ are the dimensionless aerodynamic coefficients of the control surfaces found in [28].

2.3.3. *Tilting propellers*

The airship has two independently controlled vectored tilting propellers as depicted in Fig. 2 and a third one on the stern which is unused during stratospheric cruise phase.

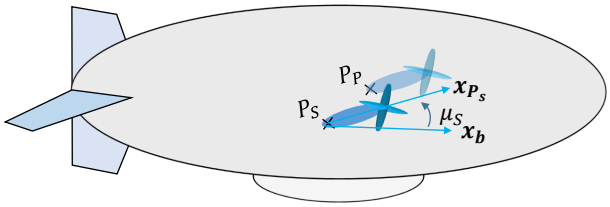


Fig. 2. Airship cruise propellers

The forces and moments generated by the propellers are:

$$\begin{pmatrix}\mathbf{f}_{CP}\\ \mathbf{m}_{CP}\end{pmatrix}_{\text{prop}} = T_{\max}\times \begin{pmatrix} \tau_p\cos\mu_p + \tau_s\cos\mu_s\\ 0\\ -(\tau_p\sin\mu_p + \tau_s\sin\mu_s)\\ d_y(\tau_p\sin\mu_p - \tau_s\sin\mu_s)\\ d_z(\tau_p\cos\mu_p + \tau_s\cos\mu_s) + d_x(\tau_p\sin\mu_p + \tau_s\sin\mu_s)\\ d_y(\tau_p\cos\mu_p - \tau_s\cos\mu_s)\end{pmatrix} \tag{9}$$

where $T_{\max}$ is the maximum thrust of a propeller, τ_p and τ_s are respectively the port and starboard throttle setting and μ_p and μ_s are respectively the port and starboard propeller tilting angles and $\begin{pmatrix} d_x & d_y & d_z\end{pmatrix}^T$ and $\begin{pmatrix} d_x & -d_y & d_z\end{pmatrix}^T$ are the positions of the starboard propeller and port propeller in the body frame respectively.

2.3.4. *Virtual control inputs*

Equation (9) is non-linear. Hence, to rewrite the system as a non-linear affine in control system 6, a virtual inputs formulation is used [18].

Instead of the tilting angles and throttle settings, equation 9 can be expressed using the propellers thrust along x_b and z_b axes: T_{xp}, T_{xs} and T_{zp}, T_{zs} as:

$$\begin{pmatrix}\mathbf{f}_{CP}\\ \mathbf{m}_{CP}\end{pmatrix} = \begin{pmatrix} 1 & 1 & 0 & 0\\ 0 & 0 & 0 & 0\\ 0 & 0 & 1 & 1\\ 0 & 0 & -d_y & d_y\\ d_z & d_z & -d_x & -d_x\\ d_y & -d_y & 0 & 0\end{pmatrix}\begin{pmatrix}T_{xp}\\ T_{xs}\\ T_{zp}\\ T_{zs}\end{pmatrix} \tag{10}$$

Hence, the control forces and moments in (6) becomes:

$$\mathbf{U}(t) = \begin{pmatrix}\mathbf{f}_{CP}\\ \mathbf{m}_{CP}\end{pmatrix} = \mathbf{B}\mathbf{u}(t) \tag{11}$$

where $\mathbf{B}$ is the control effectiveness matrix given by

$$B = \begin{pmatrix} 1 & 1 & 0 & 0\\ 0 & 0 & 0 & 0\\ 0 & 0 & 1 & 1\\ 0 & 0 & -d_y & d_y\\ d_z & d_z & -d_x & -d_x\\ d_y & -d_y & 0 & 0\end{pmatrix} \begin{pmatrix} 0 & 0 & 0 & 0\\ 0 & 0 & 0 & 0\\ \bar{q}S_h\widehat{C}_{z\delta_e} & \bar{q}S_h\widehat{C}_{z\delta_e} & 0 & 0\\ \bar{q}S_hL\widehat{C}_{l\delta_e} & -\bar{q}S_hL\widehat{C}_{l\delta_e} & \bar{q}S_hL\widehat{C}_{l\delta_r} & -\bar{q}S_hL\widehat{C}_{l\delta_r}\\ \bar{q}S_hL\widehat{C}_{m\delta_e} & \bar{q}S_hL\widehat{C}_{m\delta_e} & 0 & 0\\ 0 & 0 & \bar{q}S_hL\widehat{C}_{n\delta_r} & \bar{q}S_hL\widehat{C}_{n\delta_r}\end{pmatrix} \tag{12}$$

and $\mathbf{u}$ is the control inputs vector given by

$$\mathbf{u} = \begin{pmatrix} T_{xp} & T_{xs} & T_{zp} & T_{zs} & \delta_{eL} & \delta_{eR} & \delta_{rU} & \delta_{rB}\end{pmatrix}^T \tag{13}$$

3. Control system

This section presents the cascaded NDI/INDI control system. The outer loop controls the airship attitude using an NDI controller whilst the inner loop controls the airship body-axis velocity and angular rate using an INDI controller involving a virtual control formulation. Then, the effective airship controls are allocated using an active-set solver, respecting both the actuator position and slew rate saturation constraints.

3.1. *Control allocation*

The airship has more actuators than outputs to control, thus a strategy to allocate the control outputs is required. The control systems calculates $\mathbf{U}(t)$, so given $\mathbf{U}(t)$, the control allocation problem is to determine $\mathbf{u}(t)$. A pseudo-inverse of $\mathbf{B}$ from (11) could be computed, but airship actuators have highly different characteristics, so it is possible that some actuators will be saturating while the others

do not. This is not considered by the pseudo-inverse allocation. Hence, as in [18], an active-set algorithm is used. The active-set solver is implemented using the QCAT library [31].

The required thrusts and tilt angles are obtained back from $\mathbf{u}(t)$ and (12) using (for the port propeller and similarly for the starboard):

$$\begin{cases} T_p = \min\left(\sqrt{T_{xp}^2 + T_{zp}^2}, T_{\max}\right), \\ \mu_p = -\operatorname{atan2}(T_{zp}, T_{xp}) \end{cases} \tag{14}$$

3.2. *Velocity and angular rates control*

The inner-loop controls control the velocity and the angular rates of the airship by generating equivalent forces and moments commands. Equation (6) defines a system affine in control. Hence, nonlinear dynamic inversion can be applied to design a velocity and angular rate controller.

However, the inversion process requires a precise onboard model of the stratospheric airship aerodynamics, which is by definition uncertain. Thus, to improve the controller robustness an incremental NDI controller has been implemented [25,26]. Following the INDI principle [22], applied to the airship dynamics model (6), the incremental control input is:

$$\mathbf{\Delta U}(t_k) = \mathbf{M}_a(\mathbf{v}_D(t_k) - \dot{\mathbf{x}}_2(t_k - 1)) \tag{15}$$

where $\mathbf{\Delta U}$ is the incremental virtual control forces and moments inputs corresponding to $\mathbf{U}$, $\mathbf{v}_D$ is a proportional control law, t_k and t_{k-1} are the current time step and the previous time step, respectively.

Remark 3.1. It is valid to use directly $\mathbf{M}_a$ in the NDI equation since the mass is assumed to be slowly varying (especially relatively to the control frequency) as per Assumption 2.1.

Due to the inherent robustness properties of the incremental NDI, a simple proportional control law can be used for the five channels (the lateral velocity is excluded since the airship is under-actuated). The gains should be chosen to ensure the bandwidth separation factor between the control loop and the actuators.

3.3. *Attitude control*

The attitude control loop generates angular rates demands using the NDI method. A PID controller computes the desired Euler angles derivative commands. Then, the inverse kinematic model is applied to obtain the angular rates demands:

$$\begin{pmatrix} p_{\text{ref}} \\ q_{\text{ref}} \\ r_{\text{ref}} \end{pmatrix} = \mathbf{J}^{-1}(\boldsymbol{\eta})\mathbf{v}_E(\boldsymbol{\eta}) \tag{16}$$

where $\mathbf{v}_E$ is a proportional integral derivative control law, $\mathbf{J}^{-1}$ is the inverse of the angular rates transformation matrix.

4. Guidance system

In this section, the nonlinear dynamic inversion guidance algorithm is presented. Starting from the definition of the reference trajectory and using a simplified kinematic model, the position error dynamics are derived. Since there is no analytical solution for the inversion problem, an iterative algorithm have been proposed to perform on-board the dynamics inversion, leading to the desired position error dynamics. The guidance system outputs pitch and yaw commands as well as longitudinal velocity commands to control the airship trajectory.

4.1. *Reference trajectory*

The reference trajectory, $\xi_r(t)$, is defined as in [18] and is subject to the following assumption.

Assumption 4.1. Let the reference trajectory be a function $\xi_r(t) : \mathbb{R}^+ \to \mathbb{R}^3$, class $\mathcal{D}^2$ where both $\dot{\xi}_r$ and $\ddot{\xi}_r$ are bounded.

The guidance error is expressed relative to the reference trajectory frame, defined as in [32]. The reference trajectory frame, $R_r(R, \mathbf{x}_r, \mathbf{y}_r, \mathbf{z}_r)$, is shown in Fig. 3, and whose origin R follows the reference trajectory and with axes:

- $\mathbf{x}_r$, which is aligned with the reference trajectory,
- $\mathbf{y}_r$, which is in the trajectory horizontal plane, directed to the right, and
- $\mathbf{z}_r$ wheich completes the direct orthonormalized frame.

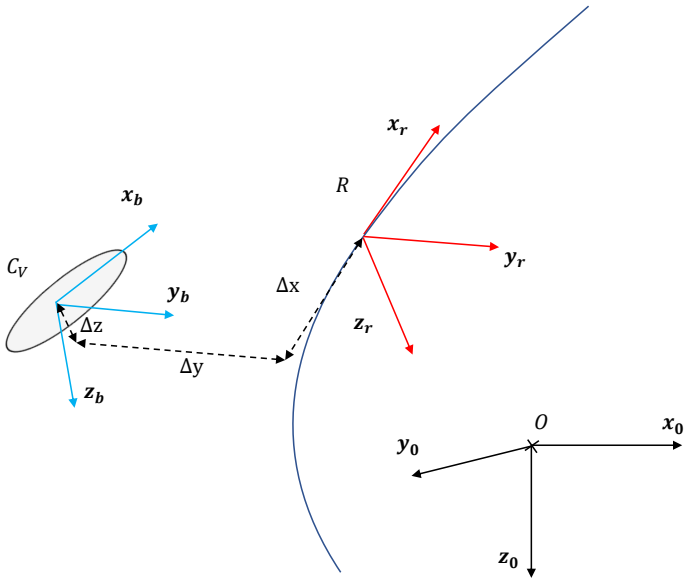


Fig. 3. Trajectory frame

The position of the origin of the reference trajectory frame relative to O, expressed in the Earth frame is:

$$\mathbf{r} = (x_{\text{ref}}\ y_{\text{ref}}\ z_{\text{ref}})^T \tag{17}$$

Then, the flight path angle and the track angle and their first order derivatives are defined, as in [32]. It must be noted that these parameters exist because the trajectory is twice differentiable, as assumed in Assumption 4.1.
The reference velocity is:

$$V_0 = \sqrt{\dot{x}_{\text{ref}}^2 + \dot{y}_{\text{ref}}^2 + \dot{z}_{\text{ref}}^2} \tag{18}$$

The flight path angle is:

$$\gamma_0 = -\arcsin \dot{z}_{\text{ref}}/V_0 \tag{19}$$

The course or track angle is:

$$\chi_0 = \text{atan2}\left(\dot{y}_{\text{ref}}, \dot{x}_{\text{ref}}\right) \tag{20}$$

Moreover, the first derivatives of the flight path and track angles are respectively:

$$\dot{\gamma}_0 = \frac{\dot{V}_0 \dot{z}_{\text{ref}} - V_0 \ddot{z}_{\text{ref}}}{V_0 \sqrt{V_0^2 - \dot{z}_{\text{ref}}^2}} \tag{21}$$

$$\dot{\chi}_0 = \frac{\dot{x}_{\text{ref}} \ddot{y}_{\text{ref}} - \dot{y}_{\text{ref}} \ddot{x}_{\text{ref}}}{\dot{x}_{\text{ref}}^2 + \dot{y}_{\text{ref}}^2} \tag{22}$$

4.2. *Guidance kinematic model*

The complete translational kinematic model inside equation (1) can be simplified using the following assumption.

Assumption 4.2. In cruise flight conditions, with or without wind:

(1) The roll angle is zero, $\phi \approx 0$. This assumption holds because the control system commands $\phi_{\text{ref}} = 0$. Note that the airship is statically stable in roll because the center of volume is higher than the center of gravity, so this assumption is valid.
(2) The lateral velocity v is not negligible and must be considered because of the wind influence.
(3) The vertical velocity w is negligible relatively to the other body velocities, $w \approx 0$. This assumption holds because the control system commands $w_{\text{ref}} = 0$. Since the airship is considered neutrally buoyant, the altitude changes are obtained by pitching up or down. At low speed or during hovering, the vertical body velocity might be non-zero, but this is out of the scope of the cruise trajectory control.

Remark 4.3. This simplified kinematic model is used for the only purpose of deriving the position error dynamics in Section 4.3 and the guidance algorithm in Section 4.4. The simulations are conducted using the full non-simplified 6-DOF model (1) and (5).

Consequently, following Assumption 4.2, the complete translational kinematic model (1) simplifies to:

$$\dot{\boldsymbol{\xi}} = \mathbf{R}(0, \theta, \psi)\,(u\ v\ 0)^T \tag{23}$$

which gives the simplified translational kinematic equation:

$$\dot{\boldsymbol{\xi}} = \begin{pmatrix} \cos\theta\cos\psi u - \sin\psi v \\ \cos\theta\sin\psi u + \cos\psi v \\ -\sin\theta u \end{pmatrix} \tag{24}$$

4.3. *Position error dynamics*

This section derives the position error dynamics using the simplified kinematic model (24).

The position error in the trajectory frame is:

$$\mathbf{e} = R_{R_E \to R_r}(\boldsymbol{\xi} - \mathbf{r}) = \begin{pmatrix} \Delta x \\ \Delta y \\ \Delta z \end{pmatrix} \tag{25}$$

where $R_{R_E \to R_r}$ is the rotation matrix between the Earth reference frame and the trajectory frame [19]:

$$\begin{aligned} R_{R_E \to R_r} &= R_Y(\gamma_0) R_Z(\chi_0) \\ &= \begin{pmatrix} \cos\gamma_0\cos\chi_0 & \cos\gamma_0\sin\chi_0 & -\sin\gamma_0 \\ -\sin\chi_0 & \cos\chi_0 & 0 \\ \sin\gamma_0\cos\chi_0 & \sin\gamma_0\sin\chi_0 & \cos\gamma_0 \end{pmatrix} \end{aligned} \tag{26}$$

Differentiating equation (25) gives:

$$\dot{\mathbf{e}} = R_{R_E \to R_r}(\dot{\boldsymbol{\xi}} - \dot{\mathbf{r}}) - \boldsymbol{\Omega}_r \times \mathbf{e} = \begin{pmatrix} \dot{\Delta} x \\ \dot{\Delta} y \\ \dot{\Delta} z \end{pmatrix} \tag{27}$$

where $\boldsymbol{\Omega}_r$ is the rotation vector of the trajectory frame relatively to the Earth reference frame expressed in trajectory frame [19]:

$$\boldsymbol{\Omega}_r = \begin{pmatrix} -\dot{\chi}_0 \sin\gamma_0 \\ \dot{\gamma}_0 \\ \dot{\chi}_0 \cos\gamma_0 \end{pmatrix} \tag{28}$$

The airship velocity in the trajectory frame after simplification becomes:

$$\mathbf{v}_{a_{R_r}} = R_{R_E \to R_r} \dot{\boldsymbol{\xi}} \tag{29}$$

$$\begin{aligned} &= \begin{pmatrix} \cos\gamma_0(\cos\theta\cos(\chi_0 - \psi)u + \sin(\chi_0 - \psi)v) \\ \cos\theta\sin(\psi - \chi_0)u + \cos(\psi - \chi_0)v \\ \sin\gamma_0(\cos\theta\cos(\chi_0 - \psi)u + \sin(\chi_0 - \psi)v) \end{pmatrix} \\ &\quad + \begin{pmatrix} \sin\gamma_0\sin\theta u \\ 0 \\ -\cos\gamma_0\sin\theta u \end{pmatrix} \end{aligned} \tag{30}$$

Moreover, the reference trajectory velocity in the reference trajectory frame is [32]:

$$R_{R_E \to R_r} \dot{\mathbf{r}} = \begin{pmatrix} V_0 \\ 0 \\ 0 \end{pmatrix} \tag{31}$$

$$\begin{pmatrix} \dot{\Delta}x \\ \dot{\Delta}y \\ \dot{\Delta}z \end{pmatrix} = \begin{pmatrix} \cos\gamma_0(\cos\theta\cos(\chi_0-\psi)u + \sin(\chi_0-\psi)v) + \sin\gamma_0\sin\theta u - V_0 - \dot{\chi}_0\cos\gamma_0\Delta y + \dot{\gamma}_0\Delta z \\ \cos\theta\sin(\psi-\chi_0)u + \cos(\psi-\chi_0)v + \dot{\chi}_0(\cos\gamma_0\Delta x + \sin\gamma_0\Delta z) \\ \sin\gamma_0(\cos\theta\cos(\chi_0-\psi)u + \sin(\chi_0-\psi)v) - \cos\gamma_0\sin\theta u - \dot{\gamma}_0\Delta x - \dot{\psi}_0\sin\gamma_0\Delta y \end{pmatrix} \tag{32}$$

Finally, substituting equations (26), (30) and (31) inside equation (27) leads to the position error dynamics equation (32).

The trajectory error dynamics equation (32) is similar to the result found in [32]. The main difference is that for the airship the simplified kinematic model (24) does not neglect the lateral velocity term.

Remark 4.4. Taking $v = 0$ inside second and third lines of (32) recovers the same equations as in [32].

4.4. *Nonlinear dynamic inversion*

Equation (32) expresses a nonlinear non-affine system where the states are the three position errors and the inputs are θ, ψ, u, v. The airship lateral velocity v cannot be directly controlled. Then, the guidance algorithm aims to compute $\theta_{\text{ref}}, \psi_{\text{ref}}, u_{\text{ref}}$ knowing v, enabling trajectory following by driving the errors to zero. To do so, the guidance controller uses NDI. Inverting equation (32) gives the velocity, the heading and the yaw commands.

4.4.1. *Velocity command*

$$u_{\text{ref}} = \frac{v_x + V_0 + \dot{\chi}_0\cos\gamma_0\Delta y - \dot{\gamma}_0\Delta z - \cos\gamma_0\sin(\chi_0-\psi_{\text{ref}})v}{\cos\gamma_0\cos\theta_{\text{ref}}\cos(\chi_0-\psi_{\text{ref}}) + \sin\gamma_0\sin\theta_{\text{ref}}} \tag{33}$$

4.4.2. *Heading command*

$$\psi_{\text{ref}} = \arcsin\frac{v_y - \dot{\chi}_0(\cos\gamma_0\Delta x + \sin\gamma_0\Delta z)}{\sqrt{\cos^2\theta_{\text{ref}}u_{\text{ref}}^2 + v^2}} - \operatorname{atan2}\frac{v}{\cos\theta_{\text{ref}}u_{\text{ref}}} + \chi_0 \tag{34}$$

The heading command (34) contains both a feedback term, a crab angle compensation term and a feedforward term.

Remark 4.5. Since the crab angle is a direct image of the wind influence on the airship, this guidance law will accommodate the wind effects without the need for external wind estimation.

4.4.3. *Pitch command*

$$\theta_{\text{ref}} = \arcsin\frac{v_z + \dot{\gamma}_0\Delta x + \dot{\chi}_0\Delta y\sin\gamma_0 - \sin\gamma_0\sin(\chi_0-\psi_{\text{ref}})v}{u_{\text{ref}}\sqrt{\cos^2\chi_0 + \sin^2\gamma_0\cos^2(\chi_0-\psi_{\text{ref}})}} + \operatorname{atan2}\frac{\sin\gamma_0\cos(\chi_0-\psi_{\text{ref}})}{\cos\gamma_0} \tag{35}$$

This contains both a feedback term and a feedforward term: if $\chi_0 \approx \psi_{\text{ref}}$ then the second term becomes γ_0, the reference flight path angle.

4.4.4. *Internal law*

The error dynamics equation (32) relies on Assumption 4.2 that may not be perfectly respected in practise. Thus to remove any potential static errors an integral term is used inside the control law. To improve stability, a derivative term has been added to obtain a PID internal law.

4.4.5. *Iterative nonlinear dynamic inversion*

It is clear from equations (33), (34) and (35) that $u_{\text{ref}}, \theta_{\text{ref}}, \psi_{\text{ref}}$ depends on each other, implying that the inversion is not complete. Therefore, as in [32], one can make a simplification enabling one shot inversion. Such simplification may rely on the assumption that $\theta_{\text{ref}} \approx \gamma_0$ for equations (33) and (34) and that $u_{\text{ref}} \approx V_0$ for equation (34). But such an assumption is not valid when both the horizontal and vertical error corrections are large and when the wind speed is large, which is often the case at high altitude.

Consequently, an iterative algorithm is proposed and is listed in Algorithm 1. From an initial guess $u_{\text{ref}}^{\text{res}} = V_0, \theta_{\text{ref}}^{\text{res}} = \gamma_0, \psi_{\text{ref}}^{\text{res}} = \chi_0$ (corresponding to the expected parameters if there is no position error and no wind), the algorithm uses (33), (34) and (35) for determining iteratively until convergence $u_{\text{ref}}, \theta_{\text{ref}}, \psi_{\text{ref}}$.

Remark 4.6. In practise, only a small number of iterations are required to converge.

Algorithm 1 Iterative NDI

Initialization: $\psi_{\text{ref}}^{\text{res}} \leftarrow \chi_0$, $u_{\text{ref}}^{\text{res}} \leftarrow V_0$, $\theta_{\text{ref}}^{\text{res}} \leftarrow \gamma_0$
while not converged **do**
  Compute ψ_{ref}^{k} using (34) with $u_{\text{ref}}^{\text{res}}$ and $\theta_{\text{ref}}^{\text{res}}$
  Compute u_{ref}^{k} using (33) with $\theta_{\text{ref}}^{\text{res}}$ and ψ_{ref}^{k}
  Compute θ_{ref}^{k} using (35) with u_{ref}^{k} and ψ_{ref}^{k}
  Update $u_{\text{ref}}^{\text{res}} \leftarrow u_{\text{ref}}^{k}$, $\theta_{\text{ref}}^{\text{res}} \leftarrow \theta_{\text{ref}}^{k}$, $\psi_{\text{ref}}^{\text{res}} \leftarrow \psi_{\text{ref}}^{k}$
end while
Return $u_{\text{ref}}^{\text{res}}$, $\theta_{\text{ref}}^{\text{res}}$, $\psi_{\text{ref}}^{\text{res}}$

Although the presented guidance law expressed in (33), (34), (35) is similar to the guidance law proposed in [32] for path following of an aircraft, our guidance law does not make any assumption on the magnitude of horizontal and vertical error corrections and it directly takes into account the wind influence by considering its influence thought the lateral velocity v.

Fig. 4 shows the proposed guidance and control system.

5. Simulation results

This section presents the simulations results of the cascaded incremental nonlinear dynamic inversion guidance and control system. Table 1 presents the airship model main parameters.

Table 1. Airship model parameters

Parameter	Value	Parameter	Value
Cruise altitude	70 000 ft	ρ	$0.0729 kg/m^3$
m	5.4×10^4 kg	$\mu_{\max}$	90°
Volume	7.4×10^5 m^3	$T_{\max}$	10×10^3 N
L	250 m	d_x, d_y, d_z	50, 35, 5 m
D	75 m	$\delta_{e_{\max}}$	±25°
S_h	8154 m^2	$\dot{\delta}_{e_{\max}}$	80 °/s
$\widehat{C}_{z\delta_e}$	-0.080617	$\widehat{C}_{l\delta_e}$	0.011802
$\widehat{C}_{m\delta_e}$	-0.037890	$\widehat{C}_{n\delta_e}$	-0.037890

5.1. *Control system*

The control system has been assessed with and without wind, at different reference velocities and for an uncertain case where the robustness to parametric uncertainties, to a certain extent, has been shown. For all the simulations, the commands are zero roll angle and a step sequence in pitch and yaw.

5.1.1. *Nominal case with and without wind*

The first test involved two simulations at 25 m/s longitudinal velocity, without wind and with 10 m/s wind.

Remark 5.1. This wind condition is representative of the average wind speed in the stratosphere [2].

Fig. 5 shows that the attitude responses are similar for the two scenarios and the control system rejects the wind disturbance. The overshoots in pitch and yaw are insignificant and the response times are small: 40 s in yaw for a large command change of 90°. Moreover, the channels are sufficiently decoupled.

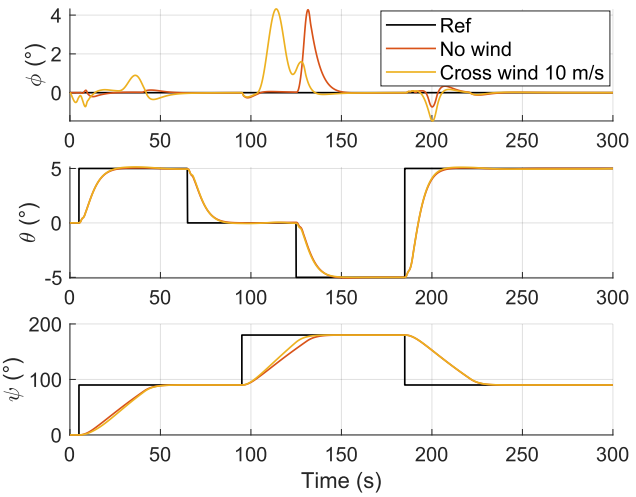


Fig. 5. Attitude, nominal case with and without wind

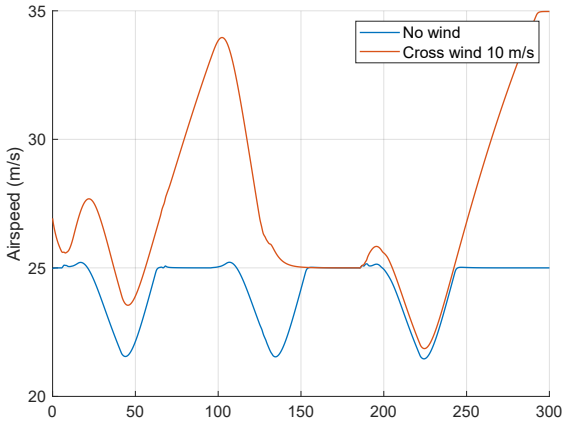


Fig. 6. Airspeed, nominal case with and without wind

Fig. 6 shows that the airspeed varies significantly when there is 10 m/s crosswind, which is expected because the command is in body velocity and not in airspeed. From about 230 s, the airship has a 90° yaw, which means it is flying into the wind so the airspeed increases to 35 m/s, while the airship maintains the 25 m/s commanded longitudinal velocity.

These results confirm that the proposed control system rejects the unknown wind perturbations.

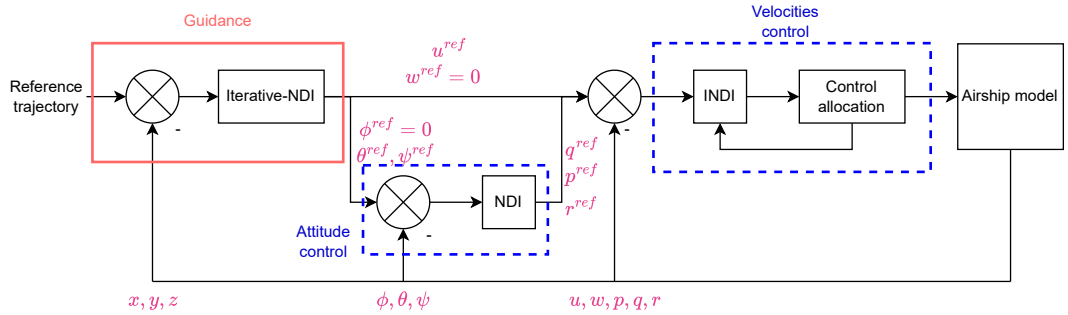


Fig. 4. Guidance and control system

5.1.2. *Airspeed influence*

The proposed control system must be effective for the whole airship flight envelope up to 40 m/s airspeed. Since the airspeed is not directly controlled, the airspeed influence is assessed via a set of seven different longitudinal velocity commands between 10 m/s and 40 m/s.

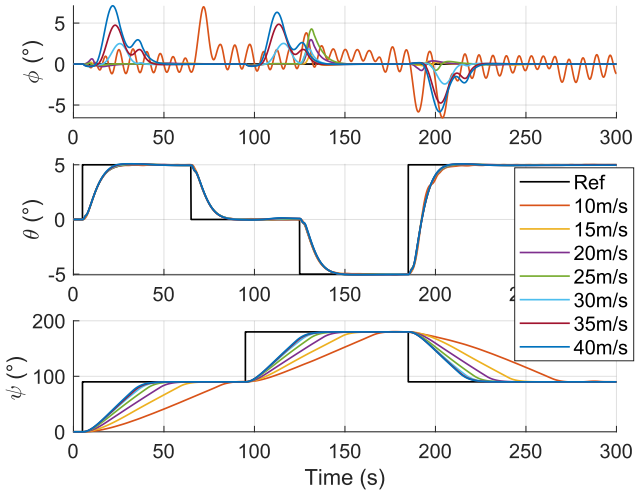


Fig. 7. Attitude response

Fig. 7 shows that airspeed has negligible impact on the roll angle, except at very low airspeed. At 10 m/s the roll angle is oscillating. The oscillations decay slowly when the manoeuvres are finished as shown in Fig. 7.

Remark 5.2. For airships, the roll mode is a second order lightly damped mode. Therefore, the control system will damp it out.

Because of the chosen weights, the control allocation prioritises the pitch and yaw channels instead of the roll channel. However, at low speeds, control efficiency is reduced, and so because of the low roll priority, roll control commands are meet less frequently: the roll mode is not damped out properly. In all cases, having roll angle oscillation mostly smaller than 5° during manoeuvres seems acceptable.

For pitch, regardless the reference velocity the response times are very similar.

On the other hand, the airspeed greatly influences the yaw response as shown by Fig. 7. This was expected because the 90° yaw manoeuvre is quite demanding for the airship, causing the controls to saturate.

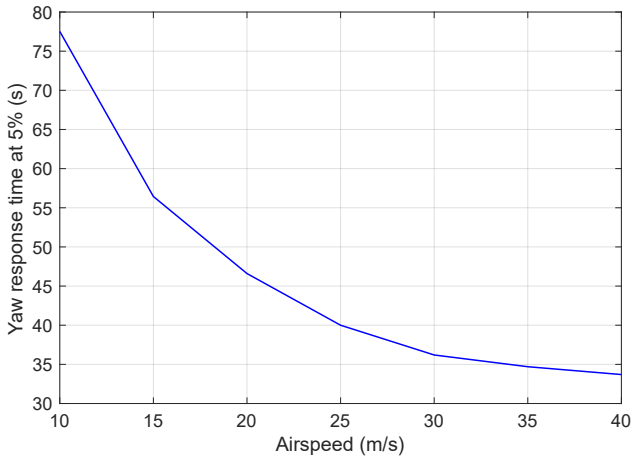


Fig. 8. Yaw response time

The lower the airspeed, the lower the response time as shown by Fig. 8. This is because the rudder yawing moment is higher at higher airspeed, then it generates a higher airship angular acceleration and hence leads to a smaller response time. It must be noted that the airship maximum yaw rate is limited by the aerodynamic damping.

Fig. 9 shows the airship longitudinal velocity u. It can be observed that the longitudinal velocity decreases during yaw turns. This decrease is larger when the initial longitudinal velocity is higher. The same trend is observed for the airspeed.

This phenomenon arises because during large yaw turns, the propeller thrust saturates and cannot keep up with the increase in drag. This is explained below.

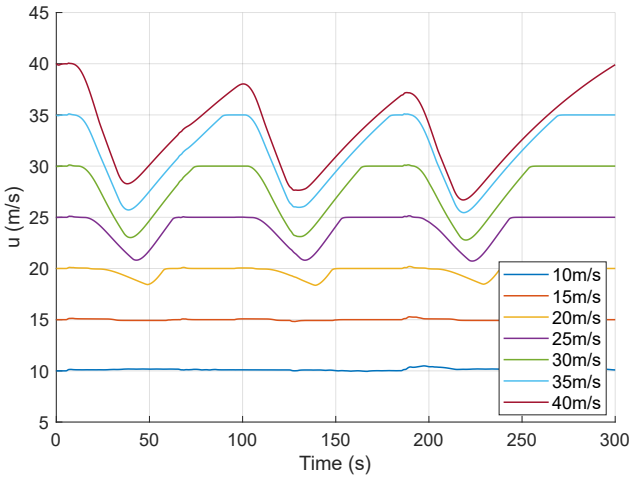


Fig. 9. Longitudinal velocity

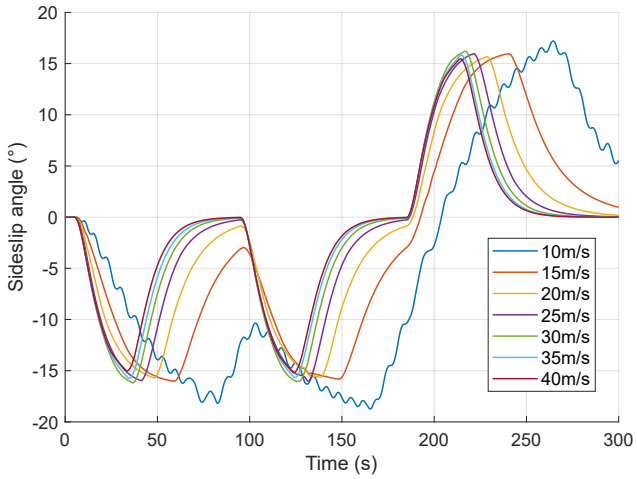


Fig. 10. Sideslip

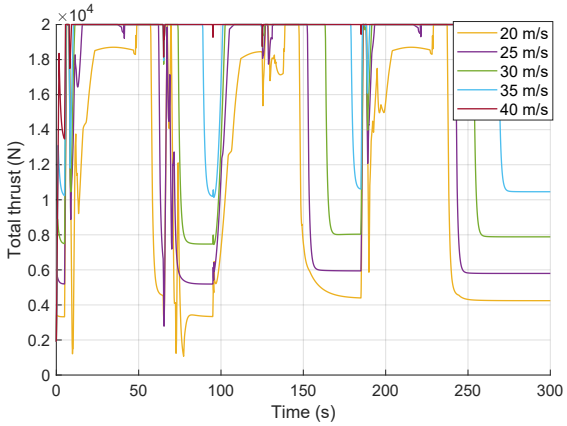


Fig. 11. Propellers total thrust

Remark 5.3. The maximum thrust of each propeller is 10,000 N (20,000 N total). This thrust was determined to compensate for the airship drag at an altitude of 70,000 feet, flying straight (without sideslip) at 45 m/s, with an appropriate margin. The maximum airspeed of 45 m/s is as per [28].

As it can be observed from Fig. 10, a large sideslip angle appears during yaw turns, as expected. This sideslip angle generates a large drag.

However, at medium to high airspeeds (20 m/s - 40 m/s), the propellers become unable to fully compensate for this increase in drag, reaching saturation as depicted in Fig. 11. It is noteworthy that due to the maximum thrust values specified in Remark 5.3, the propellers are nearly always saturating during the 40 m/s case, as shown in Fig. 12.

Following the yaw turns, the sideslip angle decreases, as shown in Fig. 10. Consequently, the drag decreases below the maximum thrust capacity of the propellers. This results in a gradual increase in the longitudinal velocity u, as expected. At the end of the maneuver, the velocity quickly returns to its commanded values with negligible overshoot across all simulations.

This concludes the analysis of the large decrease in longitudinal velocity

The 40 m/s scenario is also a relevant illustration of the efficiency of the active-set solver.

Fig. 13 illustrates the deflections of the control surfaces for this scenario. The elevator and rudder occasionally reach saturation for a few seconds, but for the most part, they remain within their operational limits. However, as demonstrated earlier in Fig. 12, the thrust of the propellers is nearly always at saturation.

Fig. 14 shows the percentage of differential thrust allocated for the 40 m/s simulation. Sometimes the differential thrust represents up to 6 % of the longitudinal thrust allocated.

Fig. 15 presents the tilting angles of the port and starboard propellers for the 40 m/s scenario. Despite the propellers being saturated as seen by Fig. 12, the solver dynamically allocates different tilting angles to the port and starboard propellers to achieve the desired differential thrust.

Following the completion of pitching and yawing maneuvers around 180 s or 250 s, the need for differential thrust ceases, and the tilting angles converge. Subsequently, the tilting angles of the propellers are exclusively utilised

to maintain the desired pitch of the airship, in coordination with the control surfaces as seen in Fig. 13 and Fig. 15.

Similar analyses could be made for other simulations.

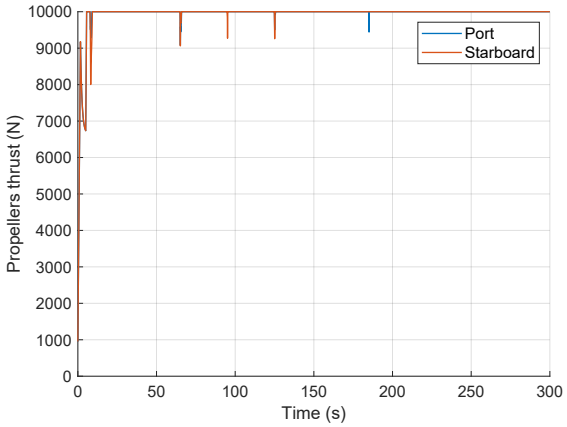


Fig. 12. Port and starboard thrust at 40 m/s

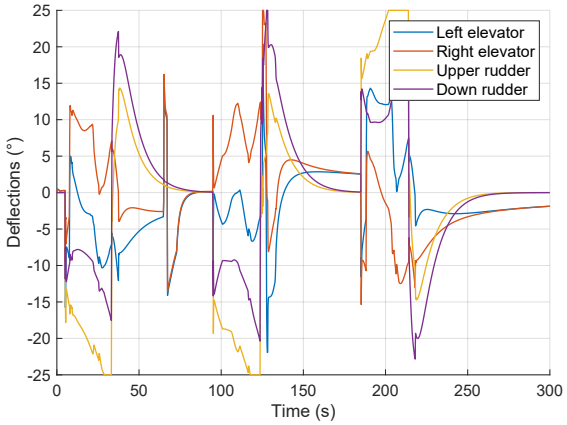


Fig. 13. Control surfaces deflections at 40 m/s

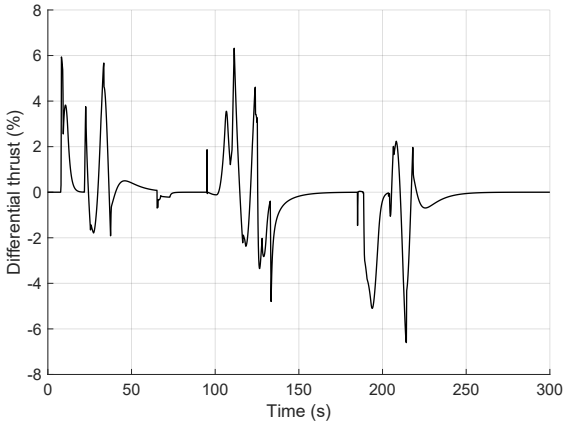


Fig. 14. Differential thrust percentage at 40 m/s

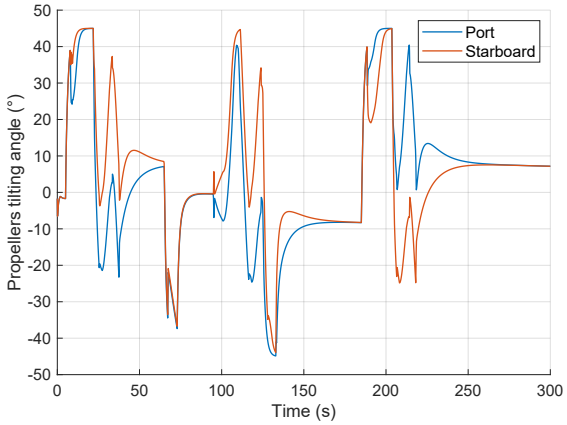


Fig. 15. Propellers tilting angle at 40 m/s

5.1.3. *Robustness analysis*

The INDI method provides enhanced robustness guarantees as discussed in [24,33] over the classical NDI method. However, it requires a precise enough estimation of the control effectiveness and mass and inertia matrices.

To verify the robustness to parametric uncertainties of the proposed control system, it is a standard engineering practise to perform Monte-Carlo simulations.

Two scenarios are considered: 25 m/s and 40 m/s longitudinal velocity. For each scenario, 300 simulations are performed in which the mass, inertia matrix, added inertia matrix and all the 24 aerodynamics coefficients (including the control surfaces coefficients) are taken randomly within independent [a] normal distributions with a standard deviation of 5% of their respective nominal value.[b]

Figures 16 and 17 show the 600 attitude responses. In most cases, the attitude response time and overshoot are acceptable. However, there are 5 exceptions from the 600 simulations. In four cases, the yaw angle has a medium overshoot of up to 20% and in one other case, the pitch response undergoes a large oscillatory deviation at 150 s. The conditions leading to these five exceptions are similar, the airship mass is approximately 10% higher than the nominal, while the pitch and yaw aerodynamic coefficients are significantly different from their nominal value.

[a] In practice there are some correlations between the model parameters, for example, mass and inertia are correlated.

[b] Then 95% of the samples will lie within a ±10% range.

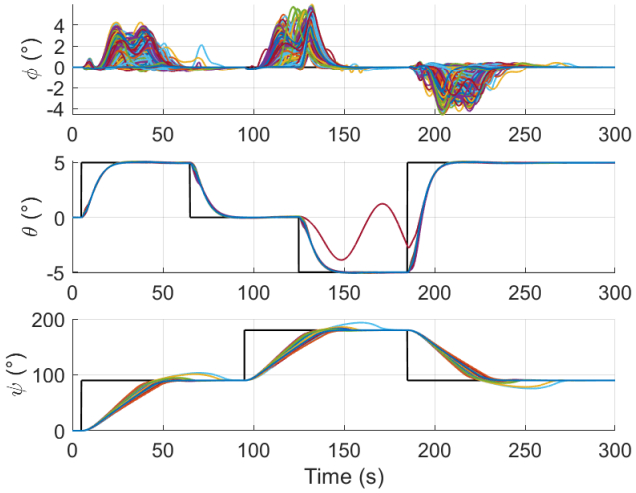


Fig. 16. Attitude, 25 m/s velocity, parametric uncertainties

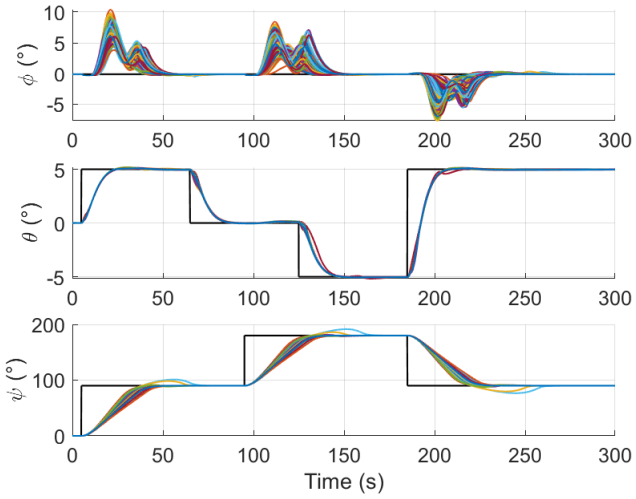


Fig. 17. Attitude, 40 m/s velocity, parametric uncertainties

If the perturbation on the mass is reduced to +8%, while keeping the other estimation errors leads to better results for the five exceptional simulations and a complete removal of the pitch angle oscillation at 150s for the 25 m/s scenario. Recalling that the mass parameter is used inside the INDI rate control loops explains why the mass parameter value must be accurate, especially if the real airship coefficients are sufficiently different than the nominal.

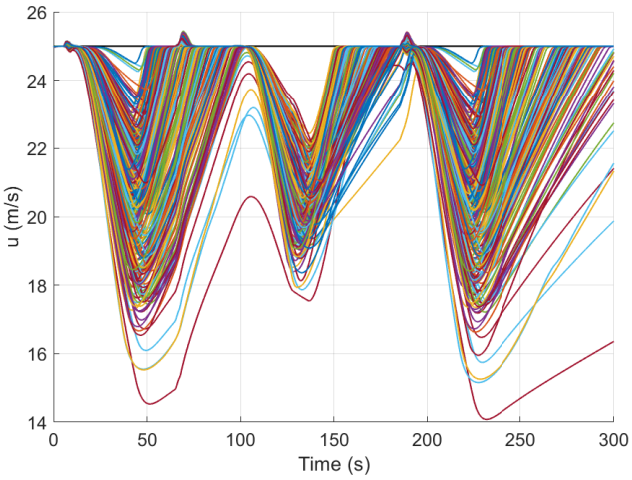


Fig. 18. Airship velocity, 25 m/s velocity reference

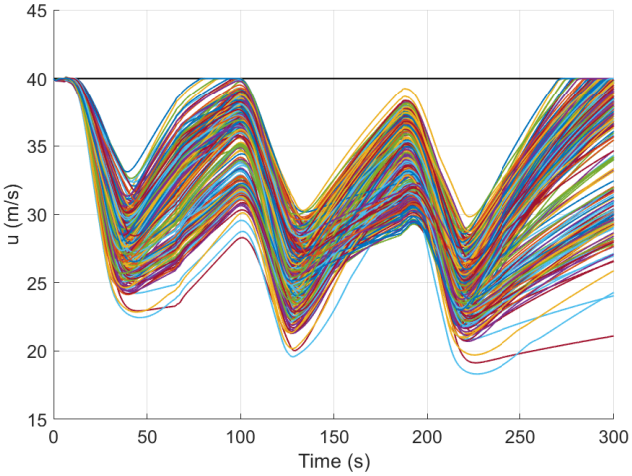


Fig. 19. Airship velocity, 40 m/s velocity reference

Figures 18 and 19 show the 600 longitudinal velocity responses. The airship velocity response is more spread than the attitude response but it is still acceptable as seen by the quantile analysis in Table 2. The velocity decrease is seen only during turns. As for the nominal case this is because during yaw turns, the large increase in sideslip induces a large increase in drag and thus reduces the velocity because the propellers saturate.

Table 2. Velocity quantiles for the maximum velocity decrease for the parametric uncertainties

Reference velocity	25 m/s			40 m/s		
Quantiles	5%	50%	95%	5%	50%	95%
Maximum decrease	28%	16%	4%	45%	35%	25%

The results show that the proposed control system is robust to parametric uncertainties in a ± 10% range. For

most of the simulations, the airship is able to conduct its manoeuvres, while meeting the overshoot and steady state error requirements.

From the simulation results and analysis the proposed control system performs well enough to be used on a stratospheric airship. The main results are:

- there is no steady state error for attitude and velocities responses,
- unknown wind perturbations, representative of the stratospheric winds, are rejected,
- the control system works well for various airspeeds,
- the control system is robust to the considered parametric uncertainties but an accurate mass estimate is important.

5.2. *Guidance system*

The control system performance has been validated in the previous subsection. Next, the proposed guidance system is assessed on two realistic trajectories: a straight-line and a helix, in presence of unknown constant or time-varying wind.

5.2.1. *Straight-line*

For the first scenario, the airship must follow a straight-line trajectory for 300 s, with an initial lateral position error of twice the airship length, i.e. 500 m. The reference longitudinal velocity is 25 m/s, and the vertical velocity is -1 m/s.

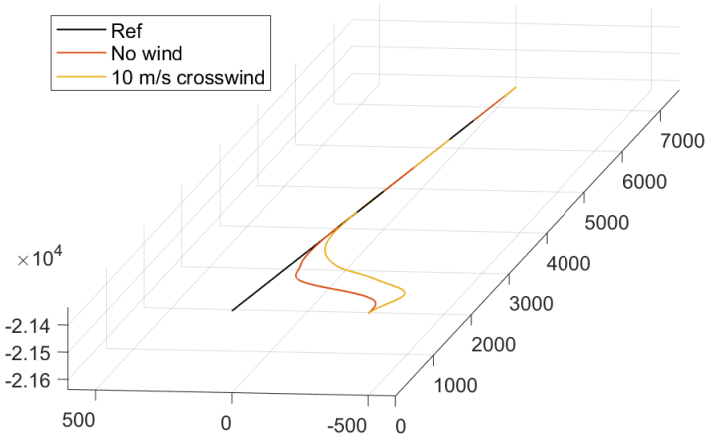


Fig. 20. Straight-line trajectory

Two test cases are presented: with 10 m/s constant wind and without wind. Fig. 20 shows the reference and airship trajectories for both cases. The airship tracks the reference closely without steady state error. Fig. 21 shows the trajectory position errors. There is an increasing lateral error for the crosswind because the airship initial heading is 0° while the wind is at 90°. Shortly after this increase, the airship compensates for the unknown wind and starts moving toward the reference trajectory.

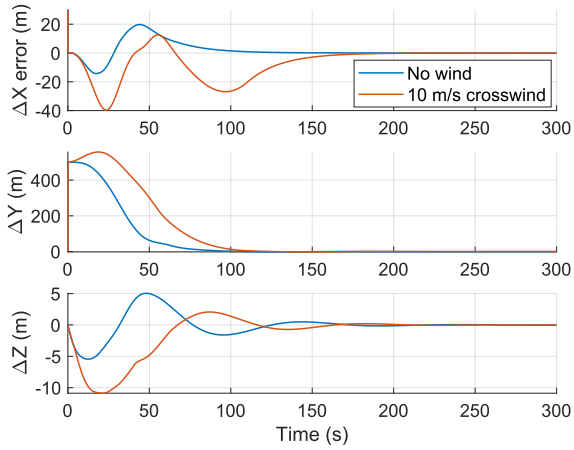


Fig. 21. Straight-line trajectory position error

5.2.2. *Helix*

For the second test case, the airship must follow a helix trajectory for 1200 s. The reference longitudinal velocity is 25 m/s, the vertical velocity is -1 m/s, and the helix has a period of 600s. Again, two simulations have been conducted with 10 m/s constant wind and without wind.

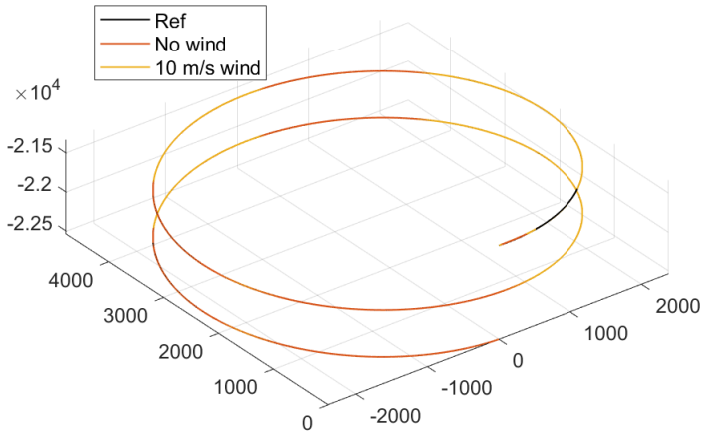


Fig. 22. Helix trajectory with and without wind

Fig. 22 shows the helix reference trajectory and the airship response with and without wind. In both cases the

airship closely tracks the reference without any steady state error. This is confirmed by the position errors displayed in Fig. 23. All errors are small with and without wind, within 2 m even for the wind disturbance case. These results demonstrate the capacity of the proposed guidance system to successfully guide the airship on the reference path, while rejecting the unknown steady wind.

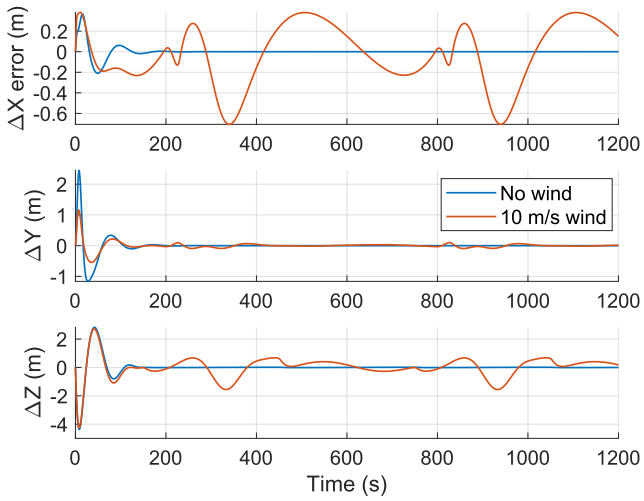


Fig. 23. Helix trajectory, error with and without wind

The good trajectory following and wind rejection properties are obtained thanks to the guidance system design. The guidance algorithm outputs attitude demands which take into account the unknown wind influence because the NDI formulation explicitly considers the lateral velocity which is an image of the wind influence.

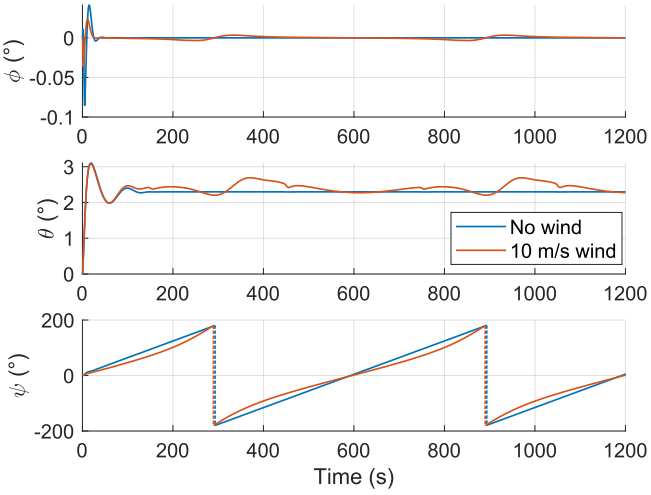


Fig. 24. Helix trajectory, attitude with and without wind

Fig. 24 shows that the attitude commands differ between the wind and no wind scenarios. This difference is more marked for the heading, where the airship generates nonzero crab angles in order to counteract the wind influence. The maximum crab angle is approximatively 25°. As expected it is obtained when the airship is flying in crosswind. Furthermore, it can be seen that the attitude references and responses are not distinguishable for both scenarios, which confirms the good perturbation rejection property of the control system seen previously in the control system results.

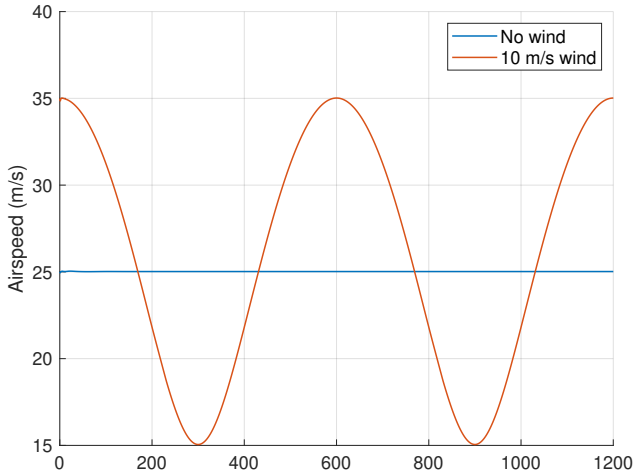


Fig. 25. Helix trajectory, airspeed with and without wind

The guidance algorithm aims to control the airship trajectory relative to the ground. This implies that the airspeed may vary significantly in case of wind. Fig. 25 shows the airspeed variation along the trajectory. Without wind the airspeed is constant and is close to the reference trajectory velocity: 25 m/s. On the other hand, with 10 m/s wind, the airspeed varies along the helix trajectory, at 0s there is a headwind and at 300s it is a tailwind.

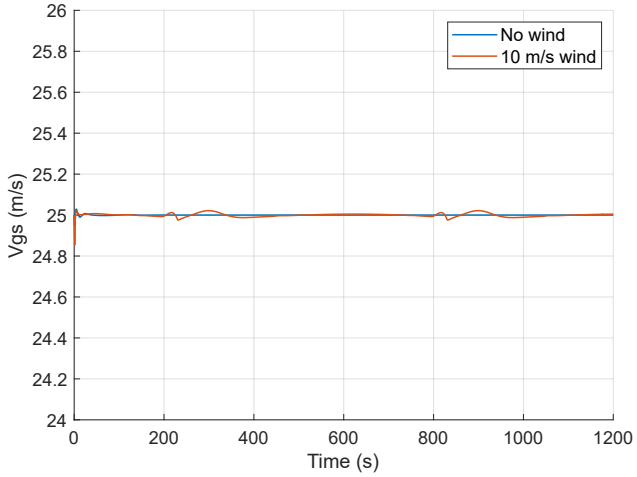


Fig. 26. Helix trajectory, ground velocity

This was expected since the airspeed itself is not controlled, which is not an issue for conventional airships since they do not require lift to sustain themselves. Airspeed protection control could be included at the expense of ground tracking accuracy. Fig. 26 shows the airship ground speed. Without or with constant wind, the ground speed tracking is great.

5.2.3. *Helix under wind gusts*

For the final scenario, the airship follows an helix trajectory with velocities ranging from 10 m/s to 40 m/s, with a radius 2500 m and a depth 600 m. The simulations duration range from 800 s to 3200 s. The wind blows from the North with a time-varying magnitude of $5 + 5\cos\left(\frac{2\pi}{T_{wind}}t\right)$ m/s where T_{wind} is the 10 s wind period.

Remark 5.4. This scenario is extreme because the maximum wind speed of 10 m/s is relatively large compared to the airship commanded ground velocity, and the wind gusts are as large as the constant wind component.

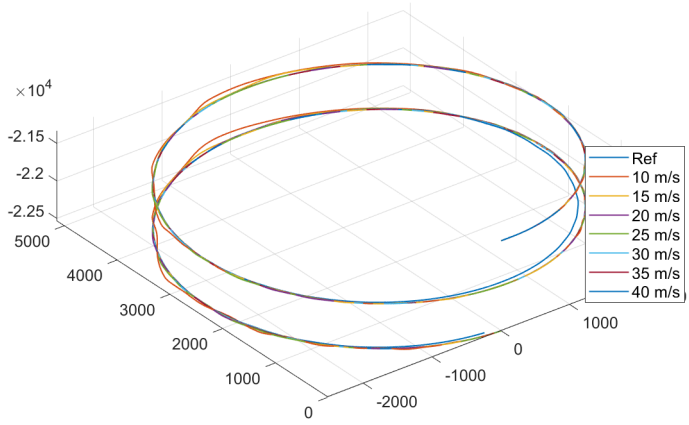


Fig. 27. Helix trajectory with wind gusts

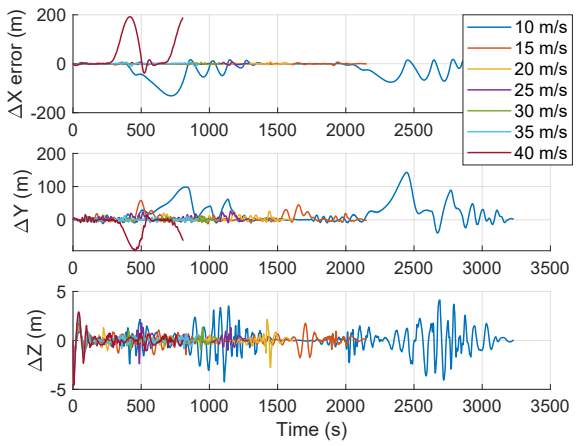


Fig. 28. Helix trajectory error with wind gusts

Fig. 27 shows that the airship is able to follow the desired path, even in presence of unknown time-varying wind gusts for all seven test cases. However, it is clear that when the commanded trajectory velocity is extremely low, the tracking performance degrades along the X and Y channels, while remaining relatively stable in the Z channel.

As seen in Fig. 28, for all velocities, the position errors are small compared to the airship size. However, for the extreme cases: 10 m/s and 40 m/s commanded ground velocity, the longitudinl position error increases significantly. For the 10 m/s this happens when the airship is flying downward the wind and hence is pushed by it: the guidance system reduces the commanded velocity accordingly but cannot reverse the thrust or go below a set threshold. For the 40 m/s this is the contrary: when the airship is flying straight to the wind, the propellers thrust saturate, leading to an increase of the longitudinal error.

6. Conclusion

An INDI approach for controlling the trajectory of a large stratospheric airship in wind is proposed and tested in simulation. A control allocation scheme is included. The guidance system inverts the simplified kinematic model of the airship to obtain the desired trajectory error linear dynamics. The wind influence is indirectly but explicitly taken into account by considering the wind induced lateral velocity of the airship.

The multiple simulation results on realistic scenarios clearly demonstrate the successful application of the proposed cascaded NDI/INDI approach to the airship trajectory following problem under various conditions, including no wind, constant wind, and wind gusts, spanning from very low to very high airspeeds. Monte-Carlo simulations confirmed that the proposed control system is robust to a certain extent to parametric uncertainties.

As previously discussed, the influence of the airship own airspeed is critical for the control system performance. Comparable or even superior performance has been achieved in prior studies such as [7,14,18–20]. Therefore, it would be worthwhile for future research to compare the results of the NDI/INDI approach with these methods across different airship airspeeds.

In [34], real flight test data of a reduced scale stratospheric airship has been presented. Even under wind gusts, the trajectory following errors (10 m) closely match the airship size (13 m). This suggests that while the presented NDI/INDI results may exhibit larger errors in the presence of wind gusts, they could still be indicative of real-world performance.

Further work could be conducted to compare the proposed solution with other control methods. In addition, further research could investigate how the INDI method behave with more representative models, in particular the difficultly of measuring angular acceleration directly. Other factors include f noisy, delayed, and biased measurements, elastic deformations of the airship structure, variation in

the centre of gravity, etc.

Data Availability Statement

Some or all data, models, or codes that support the findings of this study are available from the corresponding author upon reasonable request.

References

[1] Z. Zuo, J. Song, Z. Zheng and Q.-L. Han, A survey on modelling, control and challenges of stratospheric airships, *Control Engineering Practice* **119** (2022) p. 104979.

[2] G. D. Modica, T. Nehrkorn and T. Myers, An investigation of stratospheric winds in support of the High Altitude Airship, *13th Conference on Aviation Range and Aerospace Meteorology*, (2007).

[3] J. R. Azinheira, E. C. de Paiva, J. G. Ramos and S. S. Beuno, Mission path following for an autonomous unmanned airship, *IEEE International Conference on Robotics and Automation (ICRA 2000)*, San Francisco, CA (2000), pp. 1269–1275.

[4] D. Schmidt, Dynamic modeling, control and station-keeping guidance of a large high-altitude near-space airship, *AIAA Guidance, Navigation, and Control Conference and Exhibit*, Keystone, CO (August 2006).

[5] A. Moutinho and J. R. Azinheira, A gain-scheduling approach for airship path-tracking, *Informatics in Control Automation and Robotics: Selected Papers from the International Conference on Informatics in Control Automation and Robotics 2006*, eds. J. A. Cetto, J.-L. Ferrier, J. M. Costa dias Pereira and J. Filipe (Springer, Berlin, Heidelberg, 2008), pp. 263–275.

[6] E. C. de Paiva, F. Benjovengo and S. S. Bueno, Sliding mode control for the path following of an unmanned airship, *IFAC Proceedings Volumes* **40**(15) (2007) 221–226, 6th IFAC Symposium on Intelligent Autonomous Vehicles.

[7] Z. Zheng and Z. Wu, Global path following control for underactuated stratospheric airship, *Advances in Space Research* **52**(7) (2013) 1384–1395.

[8] Z. Zheng and W. Huo, Planar path following control for stratospheric airship, *IET Control Theory & Applications* **7**(2) (2013) 185–201.

[9] J. R. Azinheira, A. Moutinho and E. C. de Paiva, A backstepping controller for path-tracking of an underactuated autonomous airship, *International Journal of Robust and Nonlinear Control* **19**(4) (2009) 418–441.

[10] X. Wang, Z. Zuo and C. Liu, Three dimensional path-following control of an under-actuated airship, *35th Chinese Control Conference (CCC 2016)*, IEEE, Chengdu, China (July 2016), pp. 4627–4632.

[11] A. Moutinho, J. R. Azinheira, E. C. de Paiva and S. S. Bueno, Airship robust path-tracking: A tutorial on airship modelling and gain-scheduling control design, *Control Engineering Practice* **50** (2016) 22–36.

[12] Z. Zuo, L. Cheng, X. Wang and K. Sun, Three-dimensional path-following backstepping control for an underactuated stratospheric airship, *IEEE Transactions on Aerospace and Electronic Systems* **55**(3) (2018) 1483–1497.

[13] W.-X. Zhou, P.-F. Zhou, Y.-Y. Wang and D.-P. Duan, Planar path following nonlinear controller design for an autonomous airship, *Proceedings of the Institution of Mechanical Engineers, Part G: Journal of Aerospace Engineering* **233**(5) (2019) 1879–1899.

[14] L. Cheng, Z. Zuo, J. Song and X. Liang, Robust three-dimensional path-following control for an underactuated stratospheric airship, *Advances in Space Research* **63**(1) (2019) 526–538.

[15] J. Wang, X. Meng and G. Wu, Path following of the autonomous airship with compensation of unknown wind and modeling uncertainties, *Aerospace Science and Technology* **93** (2019) p. 105349.

[16] Y. Wei, P. Zhou, Y. Wang, D. Duan and Z. Chen, Virtual guidance-based finite-time path-following control of underactuated autonomous airship with error constraints and uncertainties, *Proceedings of the Institution of Mechanical Engineers, Part G: Journal of Aerospace Engineering* **235**(10) (2021) 1246–1259.

[17] S. Q. Liu, Y. J. Sang and J. F. Whidborne, Adaptive sliding-mode-backstepping trajectory tracking control of underactuated airships, *Aerospace Science and Technology* **97** (2020) p. 105610.

[18] S. Q. Liu, J. F. Whidborne and L. He, Backstepping sliding-mode control of stratospheric airships using disturbance-observer, *Advances in Space Research* **67**(3) (2021) 1174–1187.

[19] T. Souanef, J. F. Whidborne and S. Q. Liu, $\mathcal{L}_1$ adaptive path-following of airships in wind, *Unmanned Systems* (2023) Published on-line: 6 May 2023.

[20] S. Q. Liu, J. F. Whidborne, W. Z. Lyu and Q. Zhang, Observer based incremental backstepping terminal sliding-mode control with learning rate for a multi-vectored propeller airship, *Aerospace Science and Technology* **140** (2023) p. 108490.

[21] A. Moutinho and J. R. Azinheira, Path control of an autonomous airship using dynamic inversion, *IFAC Proceedings Volumes* **37**(8) (2004) 633–638, IFAC/EURON Symposium on Intelligent Autonomous Vehicles, Lisbon, Portugal, 5-7 July 2004.

[22] B. Bacon and A. Ostroff, Reconfigurable flight control using nonlinear dynamic inversion with a special accelerometer implementation, *AIAA Guidance, Navigation, and Control Conference and Exhibit*, Denver, CO (August 2000).

[23] E. J. J. Smeur, G. C. H. E. de Croon and Q. Chu, Cascaded incremental nonlinear dynamic inversion for MAV disturbance rejection, *Control Engineering Practice* **73** (2018) 79–90.

[24] R. C. van 't Veld, E.-J. Van Kampen and Q. P. Chu, Stability and robustness analysis and improvements

for incremental nonlinear dynamic inversion control, *2018 AIAA Guidance, Navigation, and Control Conference*, Kissimmee, FL (January 2018).

[25] J. R. Azinheira, A. Moutinho and J. R. Carvalho, Lateral control of airship with uncertain dynamics using incremental nonlinear dynamics inversion, *IFAC-PapersOnLine* **48**(19) (2015) 69–74, 11th IFAC Symposium on Robot Control (SYROCO 2015).

[26] A. Mansur and E. Lanteigne, Altitude trajectory control of an unmanned airship using incremental nonlinear dynamic inversion, *Canadian Society for Mechanical Engineering International Congress (CSME Congress)*, Charlottetown, PE, Canada (June 2020).

[27] S. B. V. Gomes, An investigation into the flight dynamics of airships with application to the YEZ-2A, PhD thesis, Cranfield University (1990).

[28] J. B. Mueller, M. A. Paluszek and Y. Zhao, Development of an aerodynamic model and control law design for a high altitude airship, *AIAA 3rd "Unmanned Unlimited" Technical Conference, Workshop and Exhibit*, Chicagi, IL (September 2004).

[29] E. C. de Paiva, J. R. Azinheira and J. G. Ramos, Project AURORA: infrastructure and flight control experiments for a robotic airship, *Journal of Field Robotics* (2006) 201–222.

[30] C. E. Brennen, *A Review of Added Mass and Fluid Inertial Forces* jan 1982.

[31] O. Harkegard, Efficient active set algorithms for solving constrained least squares problems in aircraft control allocation, *Proceedings of the 41st IEEE Conference on Decision and Control, 2002.*, Las Vegas, NV (December 2002), pp. 1295–1300.

[32] O. Pfeifle and W. Fichter, Cascaded incremental nonlinear dynamic inversion for three-dimensional spline-tracking with wind compensation, *Journal of Guidance, Control, and Dynamics* **44**(8) (2021) 1559–1571.

[33] S. Sieberling, Q. P. Chu and J. A. Mulder, Robust flight control using incremental nonlinear dynamic inversion and angular acceleration prediction, *Journal of Guidance, Control, and Dynamics* **33** (11 2010).

[34] Z. Zheng, W. Huo and Z. Wu, Autonomous airship path following control: Theory and experiments, *Control Engineering Practice* **21**(6) (2013) 769–788.



https://dspace.org/

Cascaded incremental nonlinear dynamic inversion trajectory following for a stratospheric airship in wind

Schneider, Leo; Souanef, Toufik; Whidborne, James F.

2025-07-01
World Scientific Publishing
https://doi.org/10.1142/s2301385025500748
Schneider L, Souanef T, Whidborne JF. (2024) Cascaded incremental nonlinear dynamic inversion trajectory following for a stratospheric airship in wind. Unmanned Systems, Volume 13, Issue 4, July 2025, pp. 1185-1202

Downloaded from a DSpace repository. https://dspace.org/